AIP | Applied Physics Letters

Graphene on nanoscale gratings for the generation of terahertz Smith-Purcell radiation

Khwanchai Tantiwanichapan, Xuanye Wang, Anna K. Swan, and Roberto Paiella

Citation: Applied Physics Letters **105**, 241102 (2014); doi: 10.1063/1.4904264
View online: http://dx.doi.org/10.1063/1.4904264
View Table of Contents: http://scitation.aip.org/content/aip/journal/apl/105/24?ver=pdfcov
Published by the AIP Publishing

Graphene on nanoscale gratings for the generation of terahertz Smith-Purcell radiation

Khwanchai Tantiwanichapan, Xuanye Wang, Anna K. Swan, and Roberto Paiella[a)]
Department of Electrical and Computer Engineering and Photonics Center, Boston University, 8 Saint Mary's Street, Boston, Massachusetts 02215, USA

(Received 21 August 2014; accepted 2 December 2014; published online 15 December 2014)

Generation of THz radiation based on the Smith-Purcell effect in graphene is investigated numerically. The specific device geometry considered involves an electrically biased single-layer sheet of graphene deposited on a periodic array of holes in a solid substrate. Rigorous electrodynamic simulations combined with a basic model of charge transport are presented, showing that technologically significant output power levels can be obtained at geometrically tunable THz frequencies. These results suggest that graphene is a uniquely suited materials platform for the demonstration of THz electron-beam radiation mechanisms in compact solid-state systems. © *2014 AIP Publishing LLC*.
[http://dx.doi.org/10.1063/1.4904264]

Despite the presence of many potential applications of high significance, to date terahertz technologies remain relatively underutilized, mostly due to the lack of practical sources.[1] Of particular importance are electrically driven solid-state emitters, which can provide unparalleled miniaturization, low power consumption, and suitability to large-scale integration. Since the THz spectrum lies at the intersection between the microwave and optical domains, techniques borrowed from both disciplines have been investigated for the generation of THz radiation in semiconductors. In photonics, THz quantum cascade lasers have been developed, which can provide high-power coherent emission at frequencies down to a few THz.[2] However, the operation of these devices is inherently limited to cryogenic temperatures, which severely limits their suitability to many applications. In microwave electronics, the extension to the THz spectrum of traditional device concepts based on charge oscillations under static bias conditions (such as resonant tunneling diodes, transit-time devices, and Gunn diodes) has been investigated. However, the output power of these devices is generally found to decrease rapidly as the oscillation frequency is extended beyond 1 THz.[1]

An alternative radiation mechanism (which has received much less attention so far in the context of THz optoelectronics) involves the use of charges under uniform rectilinear motion in the presence of a periodically modulated dielectric environment. This effect was discovered by Smith and Purcell in 1953, through the measurement of visible light emission from a high-energy electron beam traveling near a metallic grating in vacuum.[3] Its observation was initially explained in terms of the image charges induced in the metal by the electron beam, which undergo periodic angular motion due to the periodically corrugated metal surface and therefore can radiate. More rigorously, the underlying radiation mechanism can be ascribed to the evanescent electromagnetic fields associated with the actual moving charges, which can be diffractively scattered by the grating into radiation.[4] The resulting emission spectrum consists of several peaks whose frequencies $\omega_{\mathbf{g}}$ are related to the reciprocal lattice vectors $\mathbf{g}$ of the grating. In the nonrelativistic limit, where the carrier velocity v is much smaller than the speed of light c, this relationship is simply $\omega_{\mathbf{g}} = \mathbf{v} \cdot \mathbf{g}$. The use of this mechanism for the generation of microwaves in vacuum-based devices (orotrons) is already well established.[5] The measurement of Smith-Purcell (SP) radiation at THz frequencies in condensed matter has also been reported, based on the two-dimensional electron gas (2DEG) of a GaAs/AlGaAs heterojunction near a periodically corrugated surface.[6] However, the output spectrum of this device was found to be extremely broad and weak, and could only be detected at cryogenic temperatures. More recently, the use of charge domains in a grating-coupled Gunn diode has also been theoretically proposed as a promising approach for the generation of THz SP radiation.[7]

In general, the pursuit of such electron-beam radiation mechanisms in traditional semiconductors is hindered by several material properties, including limited saturation velocities, low electron mobilities at room temperature, and broad thermal distribution of carrier velocities (leading to proportionally broad SP emission peaks). By virtue of its exceptional electrical properties,[8,9] graphene provides a natural candidate to overcome these limitations. Specifically, record large room-temperature mobilities above 1×10^5 cm^2/Vs can be obtained with optimized sample geometries, including suspended sheets[10,11] or sheets deposited on atomically smooth, highly inert hexagonal boron nitride (h-BN) films.[12–14] The corresponding mean free paths are on the order of 1 μm, and values exceeding 15 μm have also been measured at cryogenic temperatures.[14] In addition, due to the linear energy dispersion of graphene near the Dirac points (i.e., $E = \pm\hbar v_F k$), all carriers travel at the same relatively high speed $v_F \approx 1 \times 10^8$ cm/s. These properties, combined with the truly 2D nature of the graphene electron gas, are ideally suited to the demonstration of electron-beam radiation mechanisms in compact solid-state systems. As an illustration, recently we have investigated numerically the emission of THz light from a sinusoidally corrugated graphene sheet, due to the resulting periodic angular motion of the graphene charges.[15] In the present work, we report on a similar study

a)Electronic mail: rpaiella@bu.edu

that substantiates the promise of the SP effect in graphene for THz optoelectronics.

The specific device geometry under study is shown in Fig. 1(a), where a single-layer sheet of graphene is deposited over a 2D hole array in a solid substrate (e.g., a silicon dioxide film on silicon). In practice, an ultrathin h-BN liner could also be inserted under the graphene sheet to increase its carrier mobility. The holes are arranged on a triangular lattice with period Λ, and have cylindrical shape with depth H and diameter D fixed at 300 nm and 0.6Λ, respectively. An external voltage is applied between the source and drain contacts, producing an electric field $\hat{\mathbf{x}}E$ in the direction of a line of holes. The use of a 2D array as opposed to a 1D grating (as in the original experiment by Smith and Purcell[3]) is motivated by a fundamental difference between the electron gas in graphene and the typical electron beam of a vacuum-based device. In the latter case, all electrons can be made to travel roughly along the same direction (to within a small divergence angle). In contrast, in a condensed-matter 2DEG the carrier distribution in reciprocal space is such that, even in the presence of a bias voltage, there are carriers traveling along all possible directions on the 2DEG plane. In general, efficient SP emission is only excited by carriers traveling along the directions of the array reciprocal lattice vectors $\mathbf{g}$. Therefore, a larger fraction of the 2DEG carriers can contribute efficiently to the SP emission if a 2D array (with its multitude of reciprocal lattice vectors along several different directions) is employed.

Incidentally, the basic geometry of Fig. 1(a) (i.e., a conducting sheet parallel to a nearby grating) can also be used to produce radiation through the excitation of 2D plasmon polaritons in the conductor and their subsequent outcoupling via diffraction by the grating. This approach has also been experimentally demonstrated at THz frequencies with high-mobility semiconductor heterojunctions, where the plasmonic oscillations were excited through the decay of hot electrons injected with a large bias voltage.[16,17] A recent theoretical study has considered the same radiation mechanism in graphene,[18] with an external electron beam propagating near the graphene layer used for the efficient phase-matched excitation of THz surface plasmons. It should also be mentioned that several other techniques, mostly based on electronic interband transitions, are currently being pursued for the generation of THz light in graphene.[19–22]

In the present work, we investigate spontaneous SP radiation from electrically biased single-layer graphene. N-type samples are considered (e.g., produced via electrostatic doping), although the same results also apply to p-doped graphene. The starting point of our analysis is the current density $\mathbf{J_k} = -q\mathbf{v_k}\delta(\mathbf{r} - \mathbf{v_k}t)$ carried by a single conduction-band electron in between consecutive collisions, where $\mathbf{k}$ is the electronic wavevector (measured from the nearest Dirac point) and $\mathbf{v_k} = \mathrm{v}_F\hat{\mathbf{k}}$. Using Fourier analysis, $\mathbf{J_k}$ can be decomposed in a superposition of harmonic waves at all frequencies ω, each having wavevector component along the direction of motion given by $q_{||} = \omega/\mathrm{v}_F$.[4] Based on the linearity of Maxwell's equations, the electromagnetic fields produced by this current density can be decomposed in exactly the same fashion. Since ω/v_F is much larger than the wavenumber $q_0 = \omega/c$, the wavevector component perpendicular to the graphene plane q_z is imaginary for each term in the superposition (i.e., the electromagnetic fields produced by the electron are evanescent, as one would expect for an electron in uniform rectilinear motion). In the geometry under study, diffractive scattering by the array can then shift the in-plane wavevector of each harmonic component of these electromagnetic fields by any grating vector $\mathbf{g}$, to produce a multitude of diffracted waves. In particular, the harmonic components of frequencies near $\omega_{\hat{\mathbf{k}},\mathbf{g}} = \mathbf{v_k}\cdot\mathbf{g}$ are correspondingly scattered into radiative waves, i.e., their shifted in-plane wavevectors become smaller than q_0 so that the out-of-plane components q_z are real and radiation away from the sample is produced.

The argument just presented provides a rigorous explanation of the SP radiation mechanism, and can be used for the approximate evaluation of the output light under suitable assumptions on the grating geometry.[4] Here, we use instead a commercial simulation tool based on the finite difference time domain (FDTD) method,[23] which allows for an accurate solution under very general conditions. In order to use the built-in dipole radiation sources of the FDTD simulation engine, we take advantage of the formal equivalence between a time-varying distribution of electric dipoles [described by a polarization density $\mathbf{P}(\mathbf{r}, t)$] and the current density $\mathbf{J}(\mathbf{r}, t) = \partial\mathbf{P}(\mathbf{r}, t)/\partial t$. The radiation emitted by each electron in the graphene sheet can therefore be computed by first determining the polarization density $\mathbf{P_k}(\mathbf{r}, t)$ whose time derivative is equal to the current density $\mathbf{J_k}(\mathbf{r}, t)$ carried by the electron. The linear dipole distribution described by this polarization density can then be readily modeled in the FDTD simulations to calculate the output light.[15] Furthermore, the effect of electronic collisions can be directly included in these calculations by setting the length of the equivalent dipole distribution equal to the electron mean free path between consecutive collisions d. With this arrangement, the evanescent electromagnetic fields produced by the simulated dipole distribution are only coherently

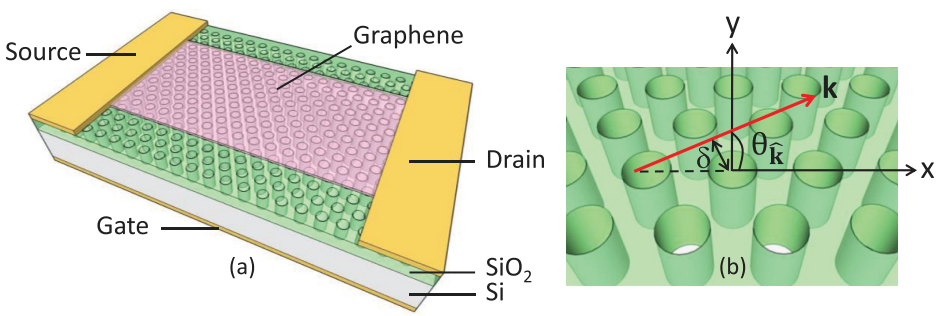

FIG. 1. (a) Schematic illustration of the sample geometry investigated in this work. (b) Close-up image of the hole array of (a), with a pictorial definition of some of the key parameters used in the simulations.

scattered by a finite number of holes in the array proportional to d/Λ, as in the case of an electron undergoing recurrent collisions in a realistic sample. Specifically, only the holes within the evanescent tail of these electromagnetic fields (i.e., within a distance on the order of $v_F/\omega_{\hat{\mathbf{k}},\mathbf{g}}$ from the simulated dipole chain) can participate in the SP radiation process.

Using this procedure, we find that the emission spectrum of each electron indeed consists of a series of peaks $P_{\hat{\mathbf{k}},\mathbf{g}}(\omega)$ at the SP frequencies $\omega_{\hat{\mathbf{k}},\mathbf{g}} = \mathbf{v_k} \cdot \mathbf{g} = v_F \hat{\mathbf{k}} \cdot \mathbf{g}$ for any reciprocal lattice vector $\mathbf{g}$. Specifically, these peaks can be clearly resolved in the FDTD spectra if the ratio d/Λ is larger than about three (and vice versa); therefore, only structures that satisfy this condition are considered in the following. The peak linewidths decrease with increasing d, as illustrated in Fig. 2, where we show representative single-electron emission spectra computed with a mean free path of 4 μm, 1 μm, and 400 nm. In each case, the array period is 100 nm and the angle $\theta_{\hat{\mathbf{k}}}$ [as defined in Fig. 1(b)] is 0° in Fig. 2(a) and 10° in Fig. 2(b). Importantly, all three values of d considered in this figure are experimentally accessible. Specifically, mean free paths of about 400 nm and 1 μm have been reported at room temperature with graphene samples on oxidized Si substrates[8] and on ultrathin h-BN films,[13,14] respectively. The higher value of 4 μm (equal to the full length of the simulated array) has been measured at about liquid-nitrogen temperature with graphene on h-BN.[14]

The two peaks observed in Fig. 2(b) for each value of d are associated with the reciprocal lattice vectors $\mathbf{g} = \mathbf{g_1}$ and $\mathbf{g_1} + \mathbf{g_2}$ (where $\mathbf{g}_1 = 2\pi(\hat{\mathbf{x}} - \hat{\mathbf{y}}/\sqrt{3})/\Lambda$ and $\mathbf{g}_2 = (4\pi\hat{\mathbf{y}})/(\sqrt{3}\Lambda)$ are the basis vectors of the array reciprocal lattice). For $\theta_{\hat{\mathbf{k}}} = 0°$, the corresponding SP frequencies are degenerate, i.e., $\omega_{\hat{\mathbf{k}},\mathbf{g}_1} = \omega_{\hat{\mathbf{k}},\mathbf{g}_1+\mathbf{g}_2}$, and only one peak is therefore obtained in Fig. 2(a). It is also apparent from these plots that the center frequency of each peak is somewhat shifted with decreasing mean free path, a behavior that is often associated with collision broadening.[24] At the same time, the total power integrated over all frequencies within each individual peak remains relatively constant with d. Additional emission features, associated with other values of $\mathbf{g}$, are also computed at higher frequencies, but with significantly lower power.

The same FDTD simulations can also be used to determine the far-field radiation properties of SP emission in

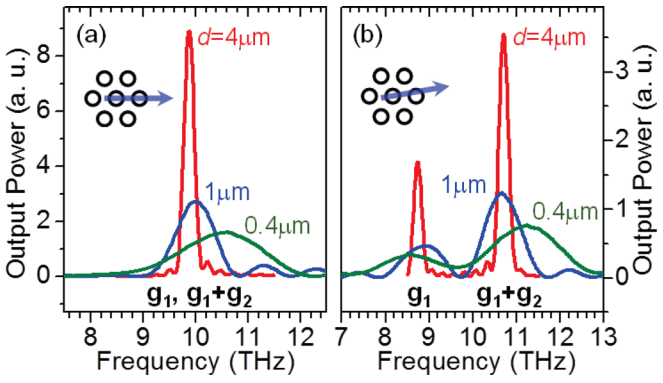

FIG. 2. Single-electron radiation spectra for different values of the mean free path d, produced by an electron traveling at an angle $\theta_{\hat{\mathbf{k}}} = 0°$ (a) and 10° (b) with respect to the x direction in the sample geometry of Fig. 1. The array period is 100 nm. The arrows in the insets show the direction of the electron velocity.

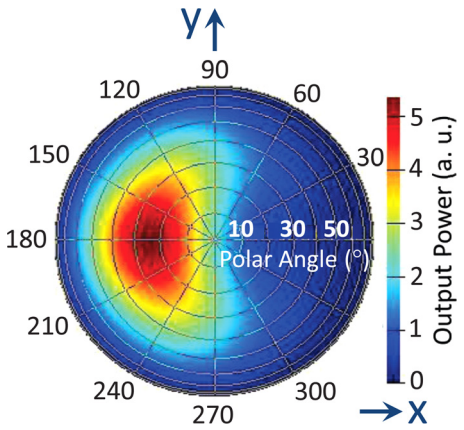

FIG. 3. Far-field radiation pattern in the array substrate produced by an electron traveling in the x direction, for $\Lambda = 100$ nm and $d = 1$ μm. The x-y coordinate system is the same as in Fig. 1(b).

graphene. To illustrate, Fig. 3 shows the radiation pattern in the plane of the substrate produced by an electron traveling along $\theta_{\hat{\mathbf{k}}} = 0°$ for $\Lambda = 100$ nm and $d = 1$ μm. The corresponding emission in the air above is significantly weaker and therefore is not considered. The key observation here is that most of the light is radiated in an oblique direction with respect to the surface normal, whose projection on the graphene plane is antiparallel to the electronic motion. The radiation pattern of Fig. 3 was computed at the frequency of peak emission of the electron under study. As the frequency is detuned from this value, the emission angle changes (consistent with the diffractive nature of the underlying mechanism), while the intensity decreases. These results are qualitatively consistent with the far-field radiation properties of SP emission from high-energy electron beams in vacuum.[4]

The total radiation output of the sample geometry under study is finally obtained by summing the single-electron contributions over all values of the wavevector $\mathbf{k}$, properly weighted by the electronic distribution function $f_{\mathbf{k}}$. Specifically, the output power spectrum is computed as follows:

$$P_{\text{tot}}(\omega) = 4 \sum_{\mathbf{k},\mathbf{g}} P_{\hat{\mathbf{k}},\mathbf{g}}(\omega) f_{\mathbf{k}} (1 - f_{\mathbf{k}-\mathbf{g}}), \tag{1}$$

where the factor of 4 accounts for the spin and valley degeneracies, $f_{\mathbf{k}}$ is the probability that the electronic initial state is occupied, and $1 - f_{\mathbf{k}-\mathbf{g}}$ is the probability that the corresponding final state after photon emission is empty. The assertion that this final state has wavevector $\mathbf{k}-\mathbf{g}$ follows from the requirement of conservation of quasi-momentum. Furthermore, if $\mathbf{g}$ is small relative to $\mathbf{k}$ (which is generally the case), the energy difference between the graphene Bloch states of wavevectors $\mathbf{k}$ and $\mathbf{k}-\mathbf{g}$ can be readily shown to be equal to $\hbar\omega_{\hat{\mathbf{k}},\mathbf{g}} = \hbar v_F \hat{\mathbf{k}} \cdot \mathbf{g}$ (i.e., the emitted photon energy) so that conservation of energy is also automatically satisfied in Eq. (1).

In order to compute $P_{\text{tot}}(\omega)$ with a practicable number of FDTD runs, the following procedure is followed. First, the FDTD simulations just described are carried out for a few values of the angle $\theta_{\hat{\mathbf{k}}}$ (i.e., the direction of $\mathbf{k}$), namely, 0°, 10°, 20°, and 30°. From these simulation results, the center frequencies, full widths at half maximum (FWHMs), and integrated powers of the corresponding single-electron emission peaks $P_{\hat{\mathbf{k}},\mathbf{g}}(\omega)$ are determined. Next, the values of the

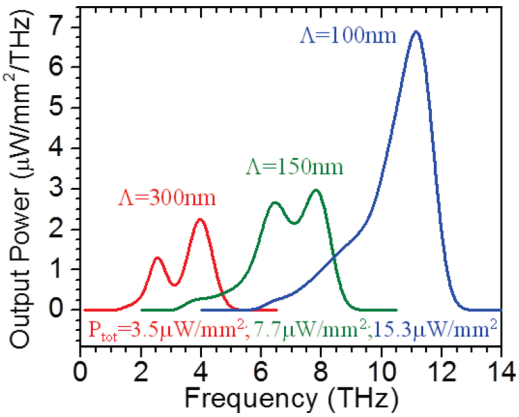

FIG. 4. Emission spectra of three graphene SP samples of different period Λ, computed with a mean free path d of 1 μm. The total output power per unit area of each structure, integrated over all frequencies, is also listed in the figure.

same parameters for all other angles $\theta_{\hat{\mathbf{k}}}$ are extrapolated using a polynomial fit and symmetry considerations. The single-electron spectra $P_{\hat{\mathbf{k}},\mathbf{g}}(\omega)$ in Eq. (1) for all values of $\theta_{\hat{\mathbf{k}}}$ are then approximated with Gaussian peaks having the correct center frequencies, FWHMs, and integrated powers (as determined with this fitting procedure). The choice of a Gaussian function is consistent with the shape of the FDTD single-electron emission peaks, and does not in any case significantly affect the shape of $P_{\text{tot}}(\omega)$. An additional complication is that the single-electron integrated output powers also depend on the displacement parameter δ defined in Fig. 1(b) [i.e., the distance from the electron trajectory to the center of a nearby reference hole]. Therefore, for each simulated value of $\theta_{\hat{\mathbf{k}}}$, different FDTD runs with representative values of δ are also carried out to find the average single-electron output power. Finally, to determine the occupation probabilities $f_{\mathbf{k}}$, we use a semiclassical model of carrier dynamics, where an externally applied electric field $\hat{\mathbf{x}}E$ has the effect of simply displacing the equilibrium Fermi-Dirac distribution function as a whole by the amount $\boldsymbol{\delta}\mathbf{k} = -\hat{\mathbf{x}}k\mathrm{v}_d/\mathrm{v}_F$, where $\mathrm{v}_d = \mu E$ is the drift velocity and μ is the mobility.[9,15]

Figure 4 shows the radiation spectra $P_{\text{tot}}(\omega)$ of three structures of different period between 100 and 300 nm, computed with a mean free path of 1 μm. A reasonably large carrier density of $5 \times 10^{12}\,\text{cm}^{-2}$ is used in these calculations, at a temperature of 300 K. For v_d, we use the experimental saturation value of 2×10^7 cm/s obtained from the high-field current-voltage characteristics of a graphene sample with carrier density of a few $10^{12}\,\text{cm}^{-2}$ at room temperature.[25] As illustrated in Fig. 2, these radiation spectra $P_{\text{tot}}(\omega)$ are derived from two $\theta_{\hat{\mathbf{k}}}$-dependent emission lines associated with diffraction by $\mathbf{g_1}$ and $\mathbf{g_1} + \mathbf{g_2}$. The latter feature is strongest for $\theta_{\hat{\mathbf{k}}} = 30^\circ$ (and equivalent directions), whereas for $\theta_{\hat{\mathbf{k}}} = 0^\circ$ the two lines are degenerate. In the 100-nm structure of Fig. 4, the two emission peaks derived from these two lines are sufficiently close to each other in frequency that they overlap (despite their relatively large quality factor), leading to particularly high peak power. In contrast, in the other structures of Fig. 4 these two peaks are clearly resolved.

The total output powers per unit area of the structures of Fig. 4, integrated over all frequencies, are listed in the figure. The key conclusion that emerges from these data is that technologically significant power levels of several $\mu\text{W/mm}^2$ can be obtained at geometrically tunable THz frequencies. Importantly, these high power levels are produced at frequencies of several THz (in fact, the smaller the array period, the higher the emission frequency and at the same time the larger the output power), contrary to the case of traditional microwave oscillators which are generally limited to frequencies below ~1 THz.[1] Combined with the inherent design simplicity and array scalability of the geometry of Fig. 1, this property makes the SP effect in graphene an attractive candidate to extend the frequency range of existing room-temperature THz sources based on compact solid-state systems. Once again, these favorable results are a direct consequence of the high mobility and large carrier velocity of single-layer graphene.

This work was supported by the National Science Foundation under Grant No. DMR-1308659. Some of the FDTD simulations were performed using the computational facilities of the Center for Nanoscale Systems at Harvard University. K. T. acknowledges support by a Royal Thai Fellowship.

[1]M. Lee and M. C. Wanke, Science **316**, 64 (2007).
[2]B. S. Williams, Nat. Photonics **1**, 517 (2007).
[3]S. J. Smith and E. M. Purcell, Phys. Rev. **92**, 1069 (1953).
[4]P. M. van den Berg, J. Opt. Soc. Am. **63**, 1588 (1973).
[5]V. L. Bratman, B. S. Dumesh, A. E. Fedotov, P. B. Makhalov, B. Z. Movshevich, and F. S. Rusin, IEEE Trans. Plasma Sci. **38**, 1466 (2010).
[6]C. Wirner, C. Kiener, W. Boxleitner, M. Witzany, E. Gornik, P. Vogl, G. Böhm, and G. Weimann, Phys. Rev. Lett. **70**, 2609 (1993).
[7]D. D. Smith and A. Belyanin, Appl. Phys. Lett. **98**, 063501 (2011).
[8]K. S. Novoselov, A. K. Geim, S. V. Morozov, D. Jiang, Y. Zhang, S. V. Dubonos, I. V. Grigorieva, and A. A. Firsov, Science **306**, 666 (2004).
[9]A. H. Castro Neto, F. Guinea, N. M. R. Peres, K. S. Novoselov, and A. K. Geim, Rev. Mod. Phys. **81**, 109 (2009).
[10]K. I. Bolotin, K. J. Sikes, J. Hone, H. L. Stormer, and P. Kim, Phys. Rev. Lett. **101**, 096802 (2008).
[11]X. Du, I. Skachko, A. Barker, and E. Y. Andrei, Nat. Nanotechnol. **3**, 491 (2008).
[12]C. R. Dean, A. F. Young, I. Meric, C. Lee, L. Wang, S. Sorgenfrei, K. Watanabe, T. Taniguchi, P. Kim, K. L. Shepard, and J. Hone, Nat. Nanotechnol. **5**, 722 (2010).
[13]A. S. Mayorov, R. V. Gorbachev, S. V. Morozov, L. Britnell, R. Jalil, L. A. Ponomarenko, P. Blake, K. S. Novoselov, K. Watanabe, T. Taniguchi, and A. K. Geim, Nano Lett. **11**, 2396 (2011).
[14]L. Wang, I. Meric, P. Y. Huang, Q. Gao, Y. Gao, H. Tran, T. Taniguchi, K. Watanabe, L. M. Campos, D. A. Muller, J. Guo, P. Kim, J. Hone, K. L. Shepard, and C. R. Dean, Science **342**, 614 (2013).
[15]K. Tantiwanichapan, J. DiMaria, S. N. Melo, and R. Paiella, Nanotechnology **24**, 375205 (2013).
[16]R. A. Höpfel, E. Vass, and E. Gornik, Phys. Rev. Lett. **49**, 1667 (1982).
[17]K. Hirakawa, K. Yamanaka, M. Grayson, and D. C. Tsui, Appl. Phys. Lett. **67**, 2326 (1995).
[18]S. Liu, C. Zhang, M. Hu, X. Chen, P. Zhang, S. Gong, T. Zhao, and R. Zhong, Appl. Phys. Lett. **104**, 201104 (2014).
[19]V. Ryzhii, M. Ryzhii, and T. Otsuji, J. Appl. Phys. **101**, 083114 (2007).
[20]F. Rana, IEEE Trans. Nanotechnol. **7**, 91 (2008).
[21]S. Boubanga-Tombet, S. Chan, T. Watanabe, A. Satou, V. Ryzhii, and T. Otsuji, Phys. Rev. B **85**, 035443 (2012).
[22]L. Prechtel, L. Song, D. Schuh, P. Ajayan, W. Wegscheider, and A. W. Holleitner, Nat. Commun. **3**, 646 (2012).
[23]FDTD Solutions, version 8.5 (Lumerical Solutions, Vancouver, 2009).
[24]G. Peach, Adv. Phys. **30**, 367 (1981).
[25]V. E. Dorgan, M. H. Bae, and E. Pop, Appl. Phys. Lett. **97**, 082112 (2010).